



RESEARCH ARTICLE

10.1029/2019JD031085

Ural Blocking Driving Extreme Arctic Sea Ice Loss, Cold Eurasia, and Stratospheric Vortex Weakening in Autumn and Early Winter 2016–2017

Key Points:

- Record-breaking blocking activity caused the cold weather over Eurasia in autumn and early winter 2016–2017
- Successive Ural blocking episodes drove the unprecedented sea ice loss over the Barents-Kara Seas in late autumn 2016
- Ural blocking episodes triggered the unseasonable weakening of the stratospheric polar vortex in November 2016

Supporting Information:

- Supporting Information S1

Correspondence to:

E. Tyrlis,
evangelos.tyrlis@mpimet.mpg.de

Citation:

Tyrlis, E., Manzini, E., Bader, J., Ukita, J., Nakamura, H. & Matei, D. (2019). Ural blocking driving extreme Arctic sea ice loss, cold Eurasia, and stratospheric vortex weakening in autumn and early winter 2016–2017. *Journal of Geophysical Research: Atmospheres*, 124, 11,313–11,329. <https://doi.org/10.1029/2019JD031085>

Received 4 JUN 2019

Accepted 15 OCT 2019

Accepted article online 31 OCT 2019

Published online 14 NOV 2019

©2019. The Authors.

This is an open access article under the terms of the Creative Commons Attribution-NonCommercial-NoDerivs License, which permits use and distribution in any medium, provided the original work is properly cited, the use is non-commercial and no modifications or adaptations are made.

Evangelos Tyrlis¹, Elisa Manzini¹, Jürgen Bader^{1,2}, Jinro Ukita³, Hisashi Nakamura⁴, and Daniela Matei¹

¹Max Planck Institute for Meteorology, Hamburg, Germany, ²Uni Climate, Uni Research and the Bjerknes Centre for Climate Research, Bergen, Norway, ³Department of Environmental Sciences, Niigata University, Niigata, Japan, ⁴Research Center for Advanced Science and Technology, The University of Tokyo, Tokyo, Japan

Abstract This study investigates the dynamics that led to the repeated cold surges over midlatitude Eurasia, exceptionally warm conditions and sea ice loss over the Arctic, and the unseasonable weakening of the stratospheric polar vortex in autumn and early winter 2016–2017. We use ERA-Interim reanalysis data and COBE sea ice and sea surface temperature observational data to trace the dynamical pathways that caused these extreme phenomena. Following abnormally low sea ice conditions in early autumn over the Pacific sector of the Arctic basin, blocking anticyclones became dominant over Eurasia throughout autumn. Ural blocking (UB) activity was four times above climatological levels and organized in several successive events. UB episodes played a key role in the unprecedented sea ice loss observed in late autumn 2016 over the Barents-Kara Seas and the weakening of the stratospheric vortex. Each blocking induced circulation anomalies that resulted in cold air advection to its south and warm advection to its north. The near-surface warming anomalies over the Arctic and cooling anomalies over midlatitude Eurasia varied in phase with the life cycles of UB episodes. The sea ice cover minimum over the Barents-Kara Seas in 2016 was not observed in late summer but rather in mid-November and December shortly after the two strongest UB episodes. Each UB episode drove intense upward flux of wave activity that resulted in unseasonable weakening of the stratospheric vortex in November. The surface impact of this weakening can be linked to the migration of blocking activity and cold spells toward Europe in early winter 2017.

1. Introduction

During autumn and early winter 2016–2017, several extreme events were observed in the Arctic cryosphere, troposphere, and stratosphere. Recurrent cold spells affected midlatitude Eurasia while exceptionally warm conditions and sea ice loss were observed over the Arctic. Additionally, an unseasonable weakening of the stratospheric polar vortex occurred in November 2016. Navarro et al. (2019) suggested that the record-breaking low precipitation over parts of western Europe in December 2016 might have occurred due to the low sea ice cover (SIC) over the Barents-Kara Seas (BKS). The Warm Arctic-Cold Continents pattern (e.g., Sun et al., 2016) was of record strength in October 2016; the cold Siberian anomaly drove an abnormally weak stratospheric vortex and negative North Atlantic Oscillation (NAO) in November–December 2016 (Tyrrell et al., 2019). A wave train in October 2016 propagated from the North Atlantic across Eurasia and eventually induced Siberian cooling and an anomalous upper level low. Constructive interference between this anomalous pattern and the planetary wave number 1 pattern resulted in enhanced upward wave propagation into the stratosphere and weakening of the polar vortex (Tyrrell et al., 2019).

The Warm Arctic-Cold Continents pattern emerged in recent decades as a result of the Arctic warming, known as Arctic Amplification (AA; e.g., Serreze & Francis, 2006) and cooling over midlatitude Eurasia and North America (e.g., Cohen et al., 2014; Horton et al., 2015; Zhang et al., 2012). Over Eurasia this pattern is referred to as the Warm Arctic-Cold Siberia/Eurasia (WACS/WACE) pattern (Mori et al., 2014, 2019). The possible existence of this pattern has stirred a major debate (Barnes & Screen, 2015; Fischer & Knutti, 2014; Palmer, 2014; Wallace et al., 2014) between studies that provided evidence supporting such a pattern (e.g., Mori et al., 2014, 2019; Kretschmer et al., 2016; Kug et al., 2015) and others that did not report significant linkages (e.g., Li et al., 2015; Screen et al., 2013). Analysis based on a large ensemble of simulations suggests

that the recently observed cooling over central Asia was probably independent to sea ice variability over the BKS but instead was caused by internal variability (e.g., McCusker et al., 2016; Ogawa et al., 2018). More recently, through a joint analysis of observations and ensemble climate model outputs, Mori et al. (2019) concluded that models are likely to underestimate the atmospheric response to sea ice variability in the BKS.

A plethora of pathways have been proposed to explain the dynamics driving the WACS (Barnes & Screen, 2015; Cohen et al., 2014). First, the weakening of the meridional near-surface temperature gradient in mid-latitudes has been thought to cause a more meandering midlatitude westerly jet that favors blocking and midlatitude cold extremes (Francis & Vavrus, 2012, 2015; Newson, 1973). However, the suggestions for a hemisphere-wide increase in blocking activity and a wavier jet in recent decades have been widely disputed (Barnes, 2013; Barnes et al., 2014). Second, modifications in baroclinicity on a hemispheric scale have been thought to modify the position and intensity of the midlatitude storm tracks. A tendency toward the negative phase of the NAO and Arctic Oscillation (AO) has been identified in modeling studies (e.g., Peings & Magnusdottir, 2014), but its robustness has been questioned (Barnes & Screen, 2015). Third, local processes that induce regional changes in storm tracks can also have impact on a hemispheric level. Anomalous turbulent fluxes under low BKS sea ice conditions in late autumn can trigger a stationary Rossby wave, which can amplify the Siberian high (Honda et al., 2009) and result in cold conditions over East Asia. A similar response was reported for a reduction of BKS sea ice by Petoukhov and Semenov (2010) and Orsolini et al. (2012). Inoue et al. (2012) showed that during low BKS sea ice years, reduced baroclinicity over the region occurs simultaneously with anticyclonic conditions over the Siberian coast and cold advection over Siberia. The link between the Arctic and lower latitudes may also be established through a stratospheric pathway (Hoshi et al., 2017; Nakamura et al., 2016; Sun et al., 2016). Sea ice loss over the BKS during late autumn or increased snowfall over Siberia during November and December may induce a midtropospheric wave pattern over Eurasia featuring a ridge over the BKS and a trough over Siberia. Enhanced upward planetary wave activity flux can subsequently weaken the stratospheric vortex in late winter (Cohen et al., 2014; Kretschmer et al., 2016). In fact, Nishii et al. (2011) showed that blocking anomalies that develop around the BKS are particularly effective in weakening the stratospheric polar vortex.

Ural blocking (UB) is an important element of the natural variability over Eurasia. It induces an anomalous circulation that results in cooling over Siberia and warming over the BKS. Luo et al. (2016b) demonstrated that UB arises from the decay of the positive phase of NAO (NAO+), with a lag of 4–7 days through a wave train propagation resembling the negative phase of the East Atlantic/West Russia pattern (Gong & Luo, 2017). The NAO+/UB regime was also found to be the optimal circulation pattern for promoting BKS warming and sea ice loss (Luo et al., 2017). Although that a clear hemisphere-wide increase in blocking activity has not been found in recent decades, a robust increase of winter blocking over central Asia (60–120° E) has been reported (Barnes et al., 2014). During the period of rapid BKS warming after 2000, more persistent UBs were favored, which were attributed to a weakening background westerly flow over midlatitude/high-latitude Eurasia (Luo et al., 2016a). Thus, the recent Arctic warming/sea ice retreat, especially over the BKS, has resulted in more persistent UB and midlatitude cold extremes.

However, resolving the directionality of causality is not a trivial task because the UB may have an amplifying effect on the Arctic warming and sea ice loss (Luo et al., 2016a, 2016b). An investigation of the role of UB as an amplifier of Arctic sea ice loss from a daily perspective revealed that sea ice decline over the BKS lags the UB peak intensity by about 4 days (Gong & Luo, 2017). In particular, the role of quasi-stationary UB for inducing more efficient BKS sea ice loss at short time scales is crucial (Chen et al., 2018). Additionally, UB anomalies, especially in November, appear to be key for driving the WACS pattern. Peings (2019) used a nudging technique to impose UB anomalies in a high-top atmospheric model. Upward planetary wave activity was found to be strong after November UB, leading to early winter stratospheric warming followed by NAO– and extreme weather events in midlatitudes during December and January. In agreement with the observational analysis by Sorokina et al. (2016), his findings do not support the argument that increased Siberia snowfall and sea ice deficit over the BKS in November can drive UB and the WACS. Instead, the atmospheric circulation related to UB can be seen as the key driver of the sea ice anomalies over the Arctic while the snow-stratosphere coupling (e.g., Henderson et al., 2018) is challenged.

The role of UB as an amplifier of sea ice loss over the BKS in November 2016 was mentioned in Chen et al. (2018). The overall role of UB in autumn and early winter 2016–2017 was not discussed in Navarro et al. (2019) and Tyrrell et al. (2019). Specifically, the impact of UB on the strength of the stratospheric polar vortex did not receive any attention. Here, we describe how all the aforementioned extremes evolved in the presence of UB. After the description of data and methods employed in this study (section 2), the evolution of the state of the Arctic cryosphere, troposphere, and stratosphere is described from a daily perspective, and all major circulation anomalies are identified (section 3). We then study the contribution of UB to the unprecedented sea ice loss observed in late autumn 2016 over the BKS (section 4) and the significant weakening of the stratospheric vortex (section 5). Finally, section 6 summarizes the pivotal role of UB in driving these extremes.

2. Data and Methods

We diagnose the evolution of the atmospheric state using variables from the ERA-Interim data set (Dee et al., 2011) that covers the period January 1979 to June 2017. These variables include mean sea level pressure, 2-m temperature (T2m), potential temperature (θ) on the 2 PVU surface, and air temperature (T), vertical pressure velocity (ω), and geopotential height and horizontal wind components (u and v) at isobaric levels. To describe the state of the Arctic cryosphere, we use SIC and Sea Surface Temperature (SST) data from the COBE data set (Hirahara et al., 2014) that covers the period January 1979 to December 2016. We construct daily-mean time series for all variables used in this study from both data sets. As a metric for the intensity of the stratospheric polar vortex, we use the mean zonal wind at 70° N and 10 hPa; we also calculate the Polar Cap Height Index (PCHI), which is defined as area-averaged geopotential height poleward of 65° N. To assess the troposphere-stratosphere interaction and the possible impact of upward propagation of planetary wave activity on the stratospheric polar vortex, we calculate the momentum budget terms with the aid of the Transformed Eulerian Mean (TEM) framework (e.g., Andrews et al., 1987; Gerber & Manzini, 2016), which requires u , v , ω , and T as an input. Here we use the upward component of Eliassen-Palm (EP) flux (F_z), as well as the eastward wind tendency due to divergence of EP flux ($U_{tend}DEPF$). These terms are two-dimensional (latitude-pressure) zonal averages and are available at daily resolution. High positive values of F_z are suggestive of intense upward wave activity flux. Negative values of the $U_{tend}DEPF$ are associated with a weakening of the stratospheric vortex. Given that F_z is a zonal mean, the specific source region of upward wave activity flux cannot be identified. For this purpose, we also calculate daily-mean poleward Eddy Heat Flux (EHF) $v'T'$ where v' and T' denote zonal anomalies. High values of poleward EHF are associated with high values of F_z .

We identify blocking with the aid of the algorithm used in Tyrllis et al. (2015). Following Berrisford et al. (2007) and Woollings et al. (2008), daily-mean fields of θ on the 2 PVU surface are used to calculate the PV- θ Blocking Index (BI) on a 5° longitude by 4° latitude grid that extends over the latitudinal band 25°–73° N. Local and instantaneous blocking is identified where the BI is positive. Large-scale blocking is identified where local and instantaneous blocking extends over a sector of at least 15° in longitude. A *blocking event* is then defined at a specific longitude when large-scale blocking is identified within 10° in longitude. A blocking event is referred to as a *blocking episode or BE* if it lasts for 4 days or longer.

In many studies UB is defined as blocking occurring over the sector 30–90° E (e.g., Chen et al., 2018) or 40–80° E (e.g., Gong & Luo, 2017; Luo et al., 2016a). However, often, the Ural sector is loosely defined and extends beyond the above mentioned domain. For example, Peings (2019) defined a UB index as the average 500-hPa geopotential height over the domain 10° W to 80° E, 45–85° N, while Luo et al. (2016b) referred to as UB some blocking events that extended until 120° E. Here, as a proxy of the overall blocking activity over an *extended Ural sector*, BI has been averaged over the sector 60–120° E, which can also serve as a measure of the strength of the upper level westerly flow over the region. Positive values of this metric are suggestive of BE occurrence somewhere within the sector. However, strong zonal flow (negative BI) in other parts of the sector may mask the contribution coming from the blocking region. The sector-mean BI value is useful for studying the timing of BE activity. For a complete assessment of UB occurrence, it should be interpreted in conjunction with the spatial coverage of the region associated with BE that is the percentage of grid points featuring BE.

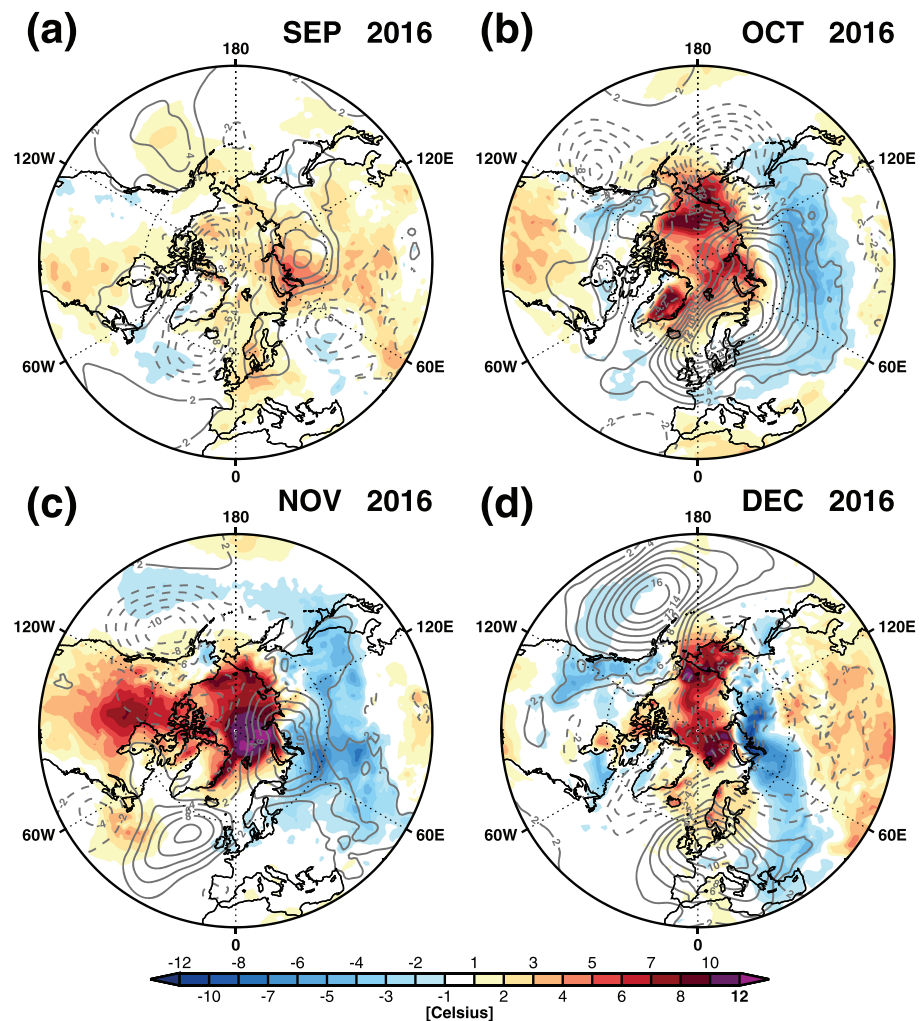


Figure 1. Monthly-mean anomalies of mean sea level pressure (contours, hPa) and 2-m temperature (shades, Kelvin) for September (a), October (b), November (c), and December 2016 (d). Contour interval is 2 hPa with solid (dashed) contours corresponding to positive (negative) values while the zero line is omitted.

3. Identification of Extremes in the Atmosphere and Arctic Cryosphere

3.1. Record-Breaking Blocking Activity Over Eurasia

During the period September–December 2016, widespread anticyclonic conditions prevailed over Eurasia accompanied by anomalously high T2m over the Arctic and low T2m over midlatitude Eurasia (Figure 1). Anticyclonic anomalies appeared in September to the east of 60° E bringing warmer than normal conditions by up to 5 ° C, over the Ural sector. In October, the anticyclones spread throughout Eurasia, especially over the sector extending from Scandinavia to the Kara Sea. In November the anticyclonic activity was mainly confined to the south and east of the BKS. In December, anticyclonic conditions persisted over Europe bringing warm and dry conditions; the mean precipitation over Europe was the lowest observed in this month since 1901 (Navarro et al., 2019).

Such dipoles of T2m anomalies are typical for blocking. Indeed, during September–December 2016, blocking activity was well above the climatological value throughout Eurasia (Figures 2a–2d). Over the sector stretching from the Urals to the Far East Asia, the surplus of BE activity relative to its climatology reached 50% in October and 30% in November. The overall UB activity in autumn 2016 was at record high levels featuring a nearly fourfold increase with respect to climatological levels; a nearly fivefold increase was recorded in October while UB activity in November 2016 was the second highest observed during the ERA-Interim period (Figure 2e). Later in winter 2017, the blocking conditions over Europe intensified (Figure S1 in the

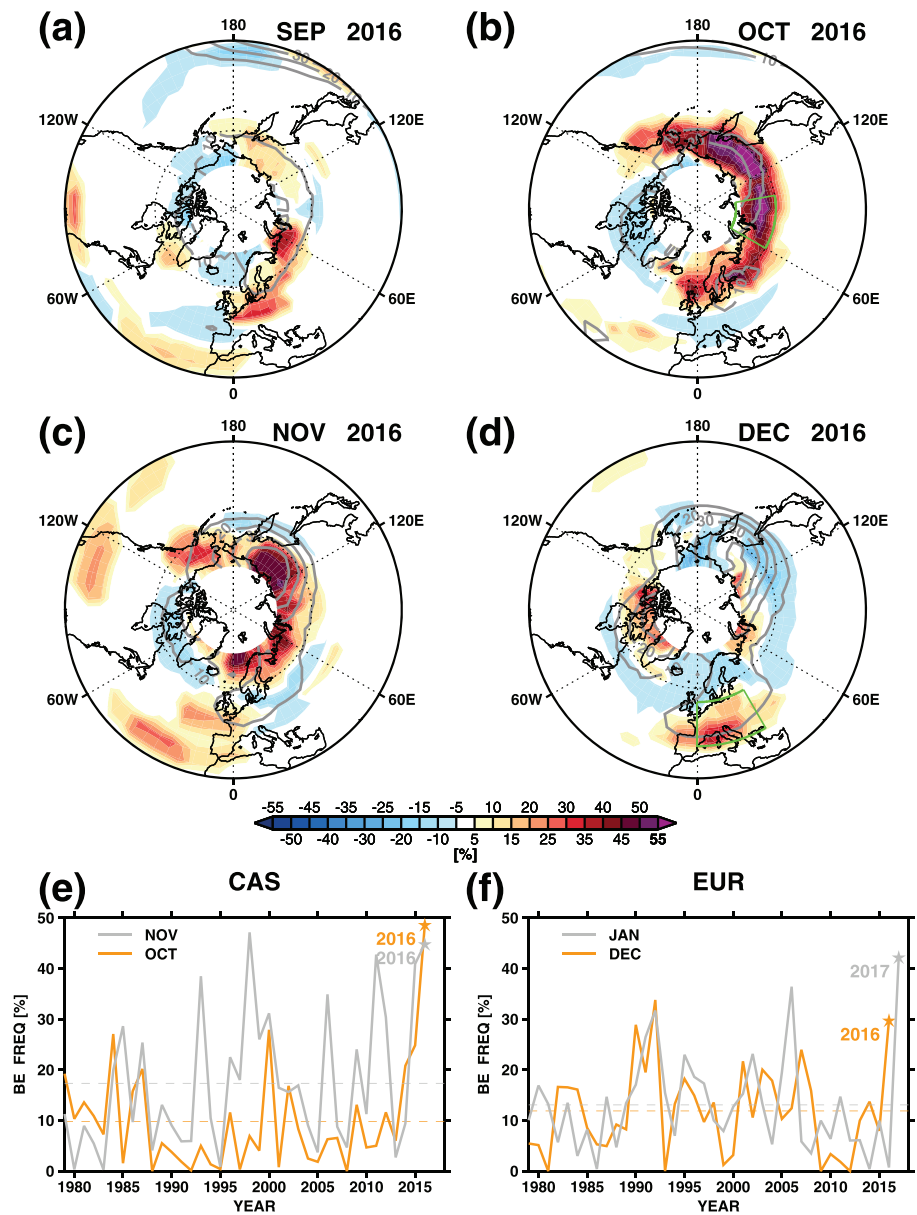


Figure 2. (a–d) Monthly-mean anomalies of Blocking Episode (BE) frequency for (a) September, (b) October, (c) November, and (d) December 2016. Anomalies are calculated with respect to the ERA-Interim climate of BE activity (contours) for the corresponding month. Interannual evolution of BE frequency (%) area averaged over a (e) Ural domain (60–100° E, 60–75° N) for October and November or a (f) European domain (0–30° E, 40–55° N) for December and January. The two domains are depicted by the green boxes in Figures 2b and 2d. Dashed lines mark the climatological values of regional BE activity for the corresponding month.

supporting information). The dry conditions there were a result of the second highest winter blocking activity observed during the ERA-Interim period. Additionally, a fourfold increase in BE frequency was observed in January (Figure 2f).

Blocking activity over Eurasia was organized as successive episodes. Over the Ural sector, four distinct BEs are identified around 1 and 22 October, 19 November, and 20 December 2016 (B1–B4 in Figure 3e). All episodes were associated with outbreaks of cold weather over CAS (south of 60° N) and warm advection off the Siberian coast (Figures 3a–3d), where monthly-mean T2m anomalies exceeded 12 ° C in November. The warming-over-cooling dipole over Asia peaked during 15–20 November 2016, when the positive and negative T2m anomalies over the BKS and CAS exceeded 25 ° C or 3 standard deviations (Figure 3c).

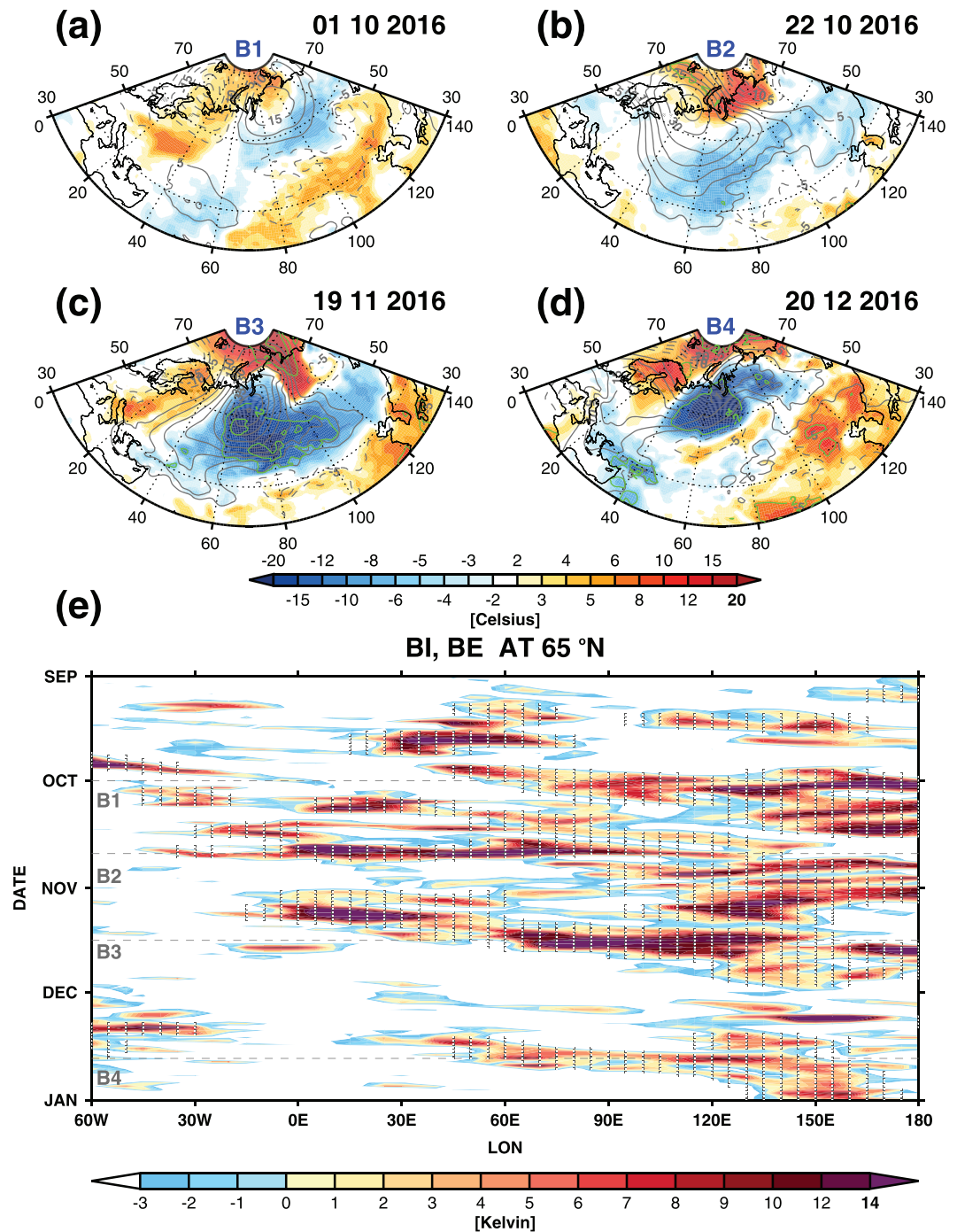


Figure 3. (a–d) Daily-mean anomalies of mean sea level pressure (contours in hPa) and 2-m temperature (T2m, shades in Kelvin) for 1 October (a), 22 October (b), 19 November (c), and 20 December (d). Panels a–d illustrate anomalies observed around the peak of Ural Blocking (UB) episodes B1–B4, respectively. Contour interval is 2 hPa with solid (dashed) contours corresponding to positive (negative) values while the zero line is omitted. Green lines represent the ratio of daily-mean T2m anomalies to the standard deviation calculated from the distribution of T2m (1979–2017) for the corresponding month. (e) Hovmöller diagram (time vs. longitude) of PV- θ Blocking Index (BI) at 65° N during the period 1 September 2016 to 31 December 2016. Positive values of BI correspond to local and instantaneous blocking. Open circles mark the occurrence of a BE at 65° N. Horizontal dashed lines mark the dates of the four major BEs B1–B4 that occurred over the Ural sector during that period.

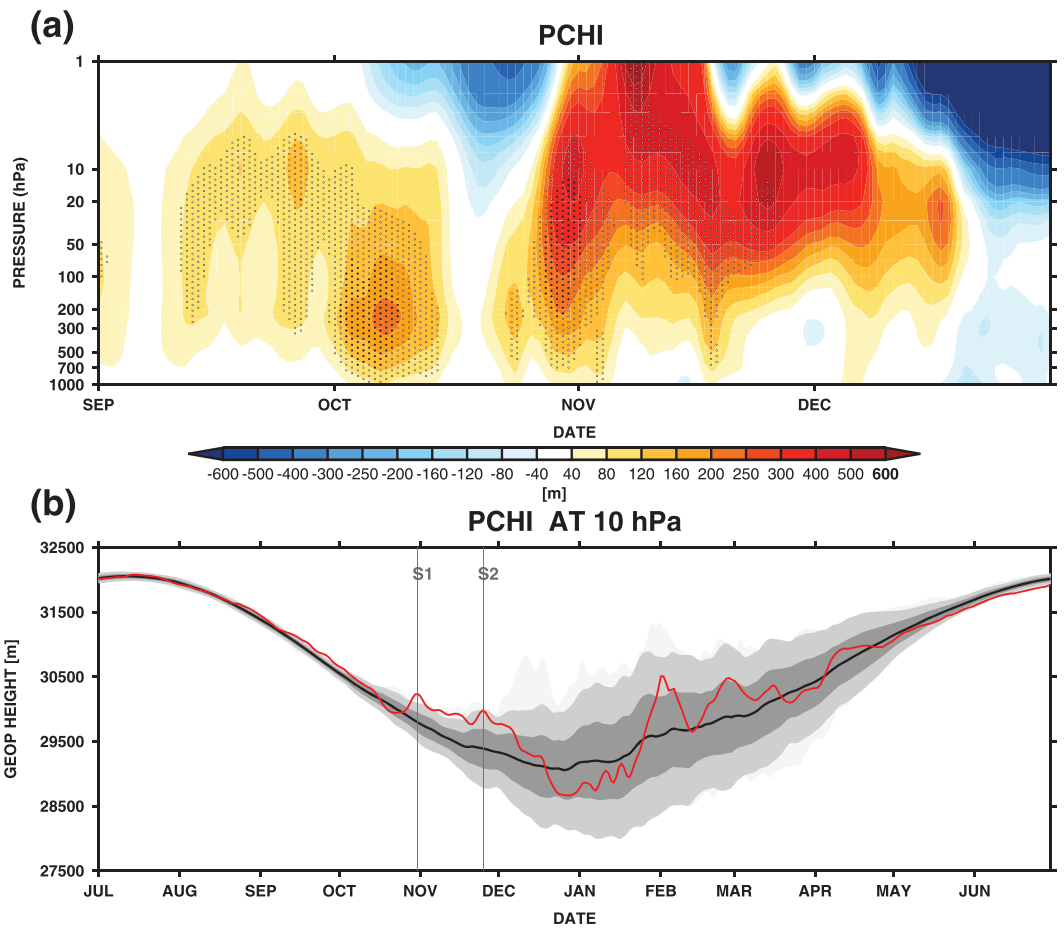


Figure 4. (a) Temporal evolution of the vertical structure of the Polar Cap Height Index (PCHI) during the period 1 September 2016 to 31 December 2016. At any given level, the PCHI is defined as the area-averaged geopotential height poleward of 65° N. The shading represents PCHI anomalies (in m) from the daily climatological cycle. Open (closed) circles delineate anomalies that exceed the levels of 2 (3) standard deviations, and thus, they mark regions where anomalies are statistically significant. (b) Temporal evolution of the PCHI (red) at 10 hPa during the period 1 July 2016 to 30 June 2017. The climatological cycle of PCHI is also depicted (black). The dark (mid) gray shading delineates the bands within 1 (2) standard deviation(s) around the mean. The light shading delineates the most extreme PCHI values observed throughout the ERA-Interim period. Vertical lines mark the dates of major episodes of stratospheric vortex weakening (S1: 31 October 2016; S2: 25 November 2016). All anomalies and statistics of the PCHI are calculated during the period 1979–2015, thus excluding 2016. Note the different time range of the horizontal axes.

The lower-latitude BEs that brought exceptionally dry weather over Europe in late December and early January are illustrated in the Hovmöller representation centered at 49° N (Figure S2a). After the strongest mid-November episode B3, each episode developed at a steadily more western location. The late-December events (E1–E3) developed over central Europe and stirred cold air advection toward southeastern Europe (Figures S3a–S3c). In early January 2017 severe cold surges affected mainly the Balkans and ranked among the most extreme cold episodes in recorded history (Anagnostopoulou et al., 2017). January events (E4–E6) occurred over western Europe and the eastern Atlantic, bringing cold spells over western Europe (Figures S3d–S3f).

3.2. Unseasonable Weakening of the Stratospheric Vortex

During September and early October 2016, positive PCHI anomalies dominated the troposphere over the Arctic basin (Figure 4a). Height anomalies were statistically significant, exceeding even 3 standard deviations in early October when the first major BE appeared over Eurasia (B1). From mid-October the height anomalies spread toward the stratosphere, resulting in a prolonged weakening of the stratospheric vortex that lasted until mid-December. This weakening is evident when exploring the evolution of the strength of the stratospheric vortex, as represented by the PCHI timeseries at 10 hPa (Figure 4b). The positive PCHI

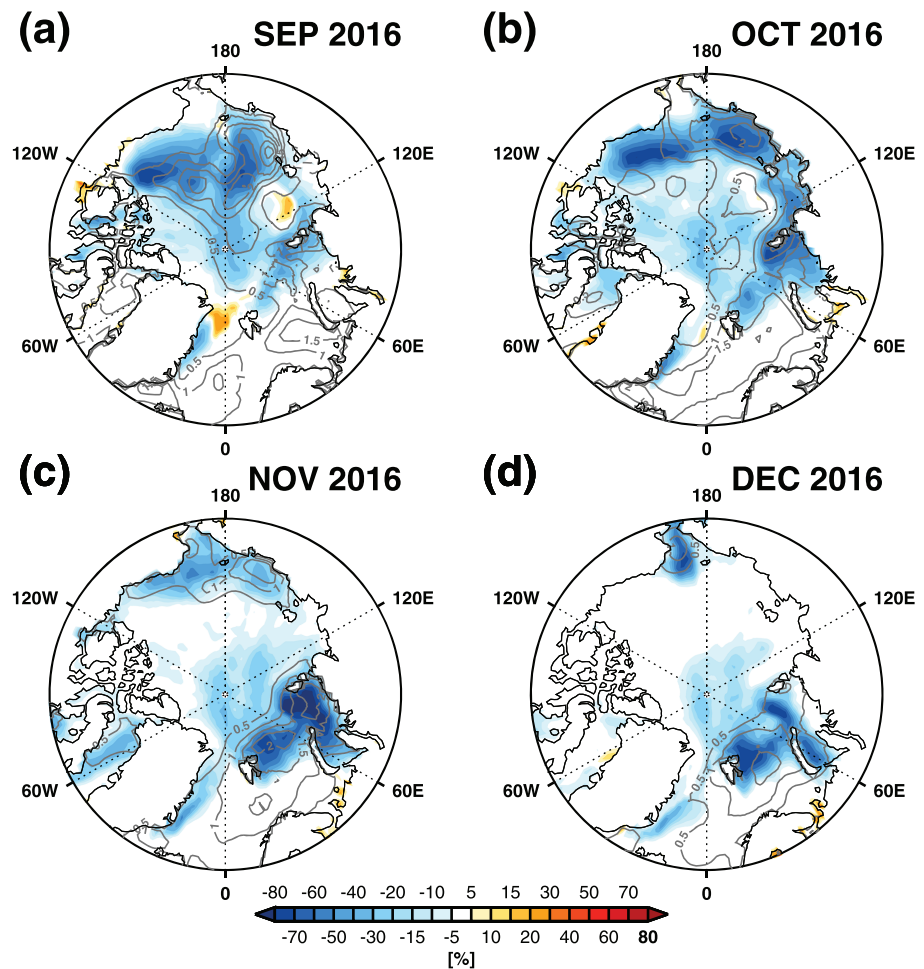


Figure 5. Monthly-mean anomalies of Sea Ice Cover (SIC; shades in %) and Sea Surface Temperature (SST; contours in Kelvin) for September (a), October (b), November (c), and December 2016 (d). Contour interval is 0.5 K with solid (dashed) contours corresponding to positive (negative) values, while the zero line is omitted.

deviation from the climatological seasonal cycle of PCHI is statistically significant for most of November, as it exceeded 2 standard deviations (midgray shade, Figure 4b).

Several peaks in PCHI are identified around 31 October and 8, 15, and 25 November 2016 corresponding to events of stratospheric vortex weakening. The ones in early and late November (S1 and S2) were the strongest; S1 was associated with the highest November PCHI values observed throughout the ERA-Interim period (Figure 4b). These episodes of stratospheric vortex weakening encompassed at least two other minor episodes in mid-November. This stratospheric anomaly was unprecedented for November, but the strength of the stratospheric vortex was near normal for the rest of the winter season. Sudden stratospheric warming events (e.g., Butler et al., 2015) often occur later in the winter, as demonstrated also by the increased variability around the climatological mean shown in Figure 4b.

3.3. Unprecedented Sea Ice Loss Over the BKS

Pronounced sea ice loss was observed over the Arctic during autumn and early winter 2016–2017. In September and October, the negative monthly-mean SIC anomalies over the East Siberia Sea (ESS), as well as the Chukchi and Beaufort Seas, exceeded 70% (Figures 5a and 5b). It is likely that this anomaly was a consequence of the extreme cyclonic activity over the Pacific sector of the Arctic basin in August 2016 (Yamagami et al., 2017). Intense summer cyclonic activity over the Arctic has been connected with low late-summer sea ice extent, as in the case of summer 2012 (Parkinson & Comiso, 2013; Zhang et al., 2013). Positive SSTs anomalies in excess of 3 °C developed over the sea ice free waters. Comparison of the monthly-mean fields of SIC for 2016 (Figures S4a and S4b), to the corresponding monthly climatology of SIC (Figures S5a and S5b),

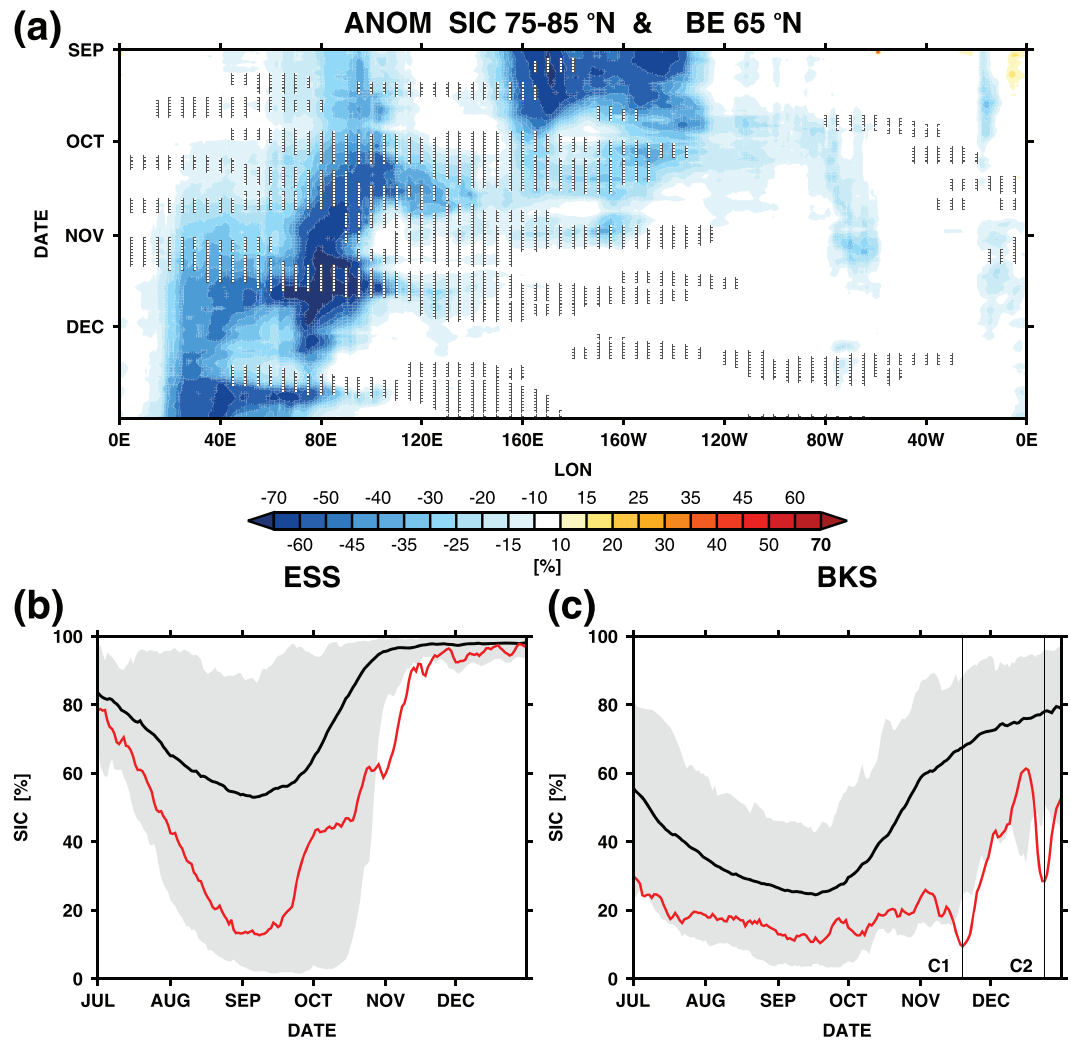


Figure 6. (a) Hovmöller diagram (time vs. longitude) showing the evolution of daily-mean anomalous Sea Ice Cover (SIC; shades in %) area averaged within the latitude band 75–85° N during the period 1 September to 31 December 2016. Open circles mark the occurrence of Blocking Episodes (BEs) at 65° N. Temporal evolution of daily-mean SIC (red) that is area averaged over the East Siberian Sea or ESS (b) and Barents-Kara Seas or BKS (c) during 2016. The daily climatological cycle (black) and most extreme SIC values (gray area) during the period 1979–2015, thus excluding 2016, are also depicted in (b) and (c). Vertical lines in (c) mark the dates of significant sea ice loss over the BKS (C1: 19 November 2016; C2: 24 December 2016).

suggests that the ESS, Chukchi, and Beaufort Seas were almost completely free of sea ice in September and October. These anomalies were embedded in a Pan-Arctic negative sea ice anomaly that is also evident in sea ice extent data from the National Snow and Ice Data Center (Figure S6). The anomalies over the ESS and Beaufort Sea peaked in early September and remained until late September (Figure 6a), while they persisted throughout October at lower latitudes near the coasts of Alaska and Siberia (Figure 5b) before freezing occurred from early November.

From mid-October a separate area of sea ice loss emerged over the BKS (Figure 6a). A detailed investigation of the evolution of the regional SIC anomalies over ESS and BKS suggests that the early autumn sea ice deficit over the ESS was striking but did not set a new record low (Figure 6b). Sea ice loss over the BKS featured two major SIC minima around 19 November and 24 December 2016 (C1 and C2 in Figure 6c), which were unprecedented in the recent observational history. In fact, the minimum of SIC for 2016 was not observed in late summer or early autumn, but rather in the second half of November. As a result, the Pan-Arctic sea ice extent in November and December 2016 reached record-breaking low levels (lower than in 2012), although during early autumn 2016, the Arctic sea ice extent was higher than in 2012 (Figure S6). The fast

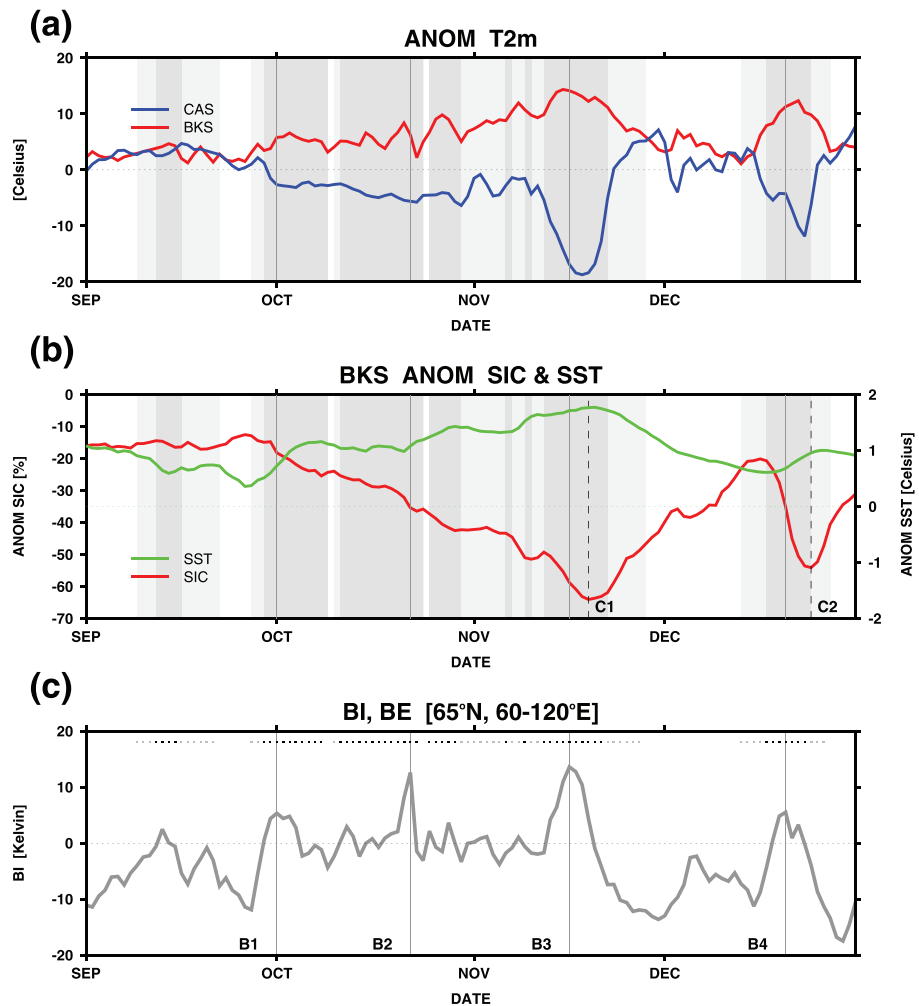


Figure 7. (a) Area-averaged 2-m temperature (T2m) anomalies over the Barents-Kara Seas (BKS, red) and central Asia (CAS, blue). (b) Area-averaged Sea Surface Temperature (SST, green) and Sea Ice Cover (SIC, red) anomalies over the BKS. (c) Blocking Index (BI) averaged over the extended Ural sector (65° N, 60–120° E). Light (heavy) gray dots or areas mark dates when Blocking Episodes (BEs) are identified in at least one grid point (in more than 50% of the population of grid points) within the Ural sector. The data shown span the period 1 September 2016 to 31 December 2016. BKS and CAS are defined by the coordinates (40–90° E, 75–85° N) and (60–100° E, 50–60° N), respectively. Vertical dashed lines in (b) mark the dates of significant sea ice loss over the BKS (C1 and C2). Vertical solid lines mark the dates of the four major BEs (B1–B4) that occurred over the Ural sector during that period.

development and retreat of C1 and C2 are suggestive of an atmospheric influence that will be investigated in the next section.

4. Role of UB in Enhancing the Sea Ice Deficit Over the BKS

In order to address the relationship between the atmospheric circulation and the sea ice anomalies, we study the evolution of daily-mean anomalies of T2m over the BKS and CAS (Figure 7a), as well as SIC and SST over the BKS (Figure 7b). Until mid-September, T2m over the BKS and CAS was up to 4 ° C higher than its climatology, while warmer SSTs by up to 1 ° C and a SIC deficit by up to 20% prevailed over the BKS. By the end of the month the anomalies gradually diminished, but this tendency reversed with the establishment of the first major Ural BE (B1, Figure 7c). Indeed, the warming over the BKS and the cooling over CAS amplified, while the sea ice deficit and the positive SST anomaly both amplified further over the BKS. The rate at which the anomalies grew accelerated as stronger and more prolonged BEs prevailed in late October and mid-November (B2 and B3). A few days after the latter event, positive anomalies of T2m and SST over the BKS reached 14 and 2 ° C, respectively, while the relative SIC deficit reached as much as 60% (C1). At

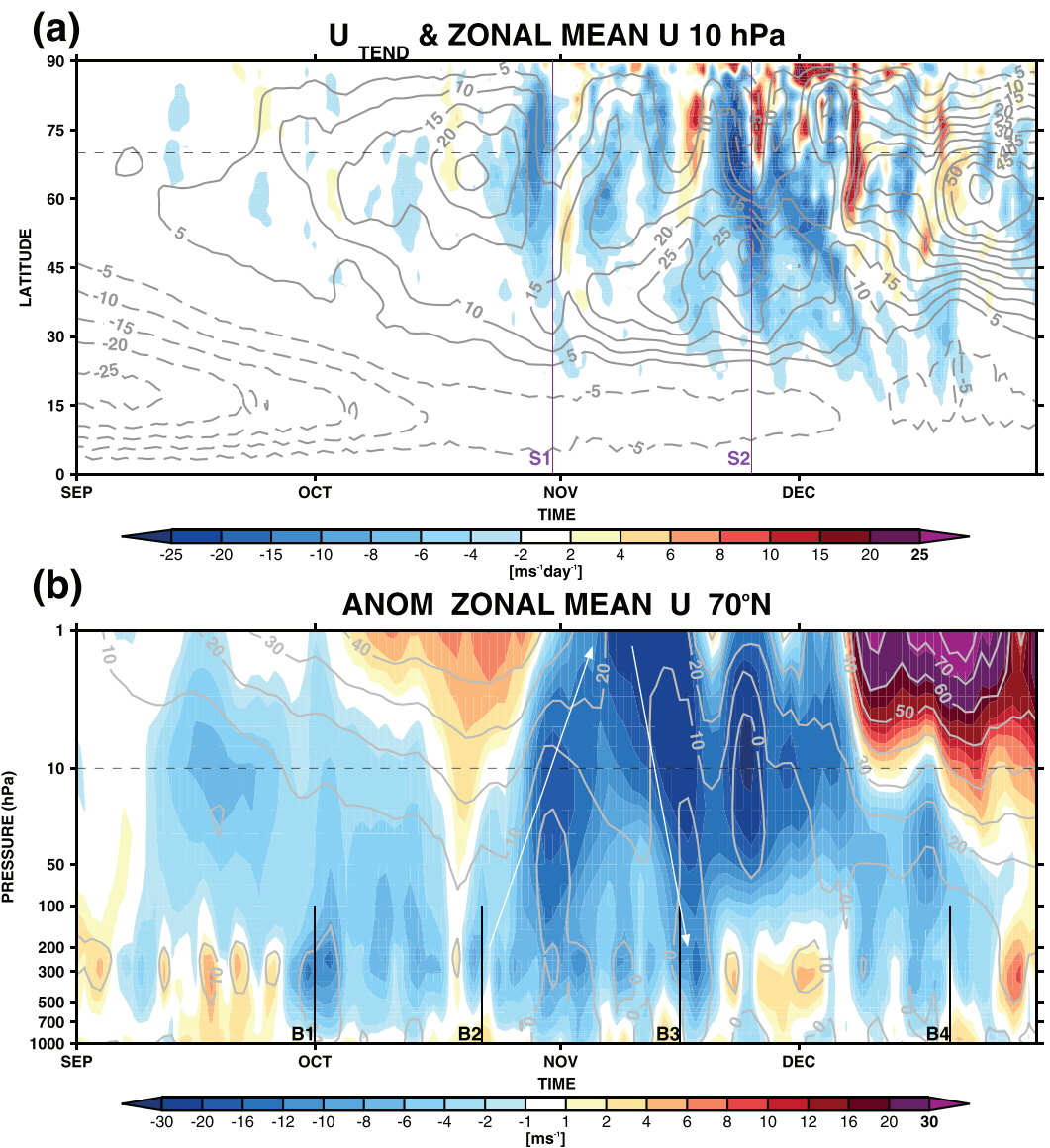


Figure 8. (a) Evolution of the latitudinal distribution of daily-mean zonal wind tendency due to divergence of Eliassen-Palm (EP) flux ($U_{tend}DEPF$, shades in $ms^{-1}day^{-1}$) and zonal-mean wind at 10 hPa (U , contours in ms^{-1}) during the period 1 September-31 December 2016. Blue shades indicate regions of easterly tendency (weakening of the westerly flow) due to EP flux divergence. Vertical lines mark the dates of the most prominent episodes of stratospheric vortex weakening (S1 and S2). (b) Evolution of the vertical distribution (zonal cross-section at $70^{\circ}N$) of the daily-mean values of zonal-mean wind (contours) and zonal-mean wind anomalies (color shades) during the period 1 September-31 December 2016. Anomalies are calculated as deviations from the daily-mean climatological cycle. The level of the cross-section in (b) is outlined with the dashed line in (a). The dashed line in (b) marks the pressure level that the latitude-time graph in (a) is visualized. Note that zonal wind tendencies are calculated in the TEM framework whereas zonal-mean wind profiles and their anomalies are taken from the ERA-Interim dataset.

the same time, T2m over CAS dropped significantly up to $20^{\circ}C$ below normal. Later, as strong westerly flow prevailed over the Ural region (Figures S3a and S3c), all anomalies in T2m and SST weakened and the sea ice recovered over the BKS. However, after the last Ural BE of late December (B4), T2m anomalies reamplified, and the SIC over the BKS grew again to 50%. The anticyclonic anomalies that formed with each of the four major BEs induced warming over the BKS and cooling over CAS (Figures 3a–3d). The dipolar T2m anomalies tended to peak within a few days after the major BEs B3 and B4 (Figure 7a).

The SIC minima C1 and C2 over the BKS lagged the peaks of the intensity of the BEs B3 and B4 by roughly 3–5 days (Figures 7b and 7c). This finding is in line with Gong and Luo (2017), who showed that UB amplifies

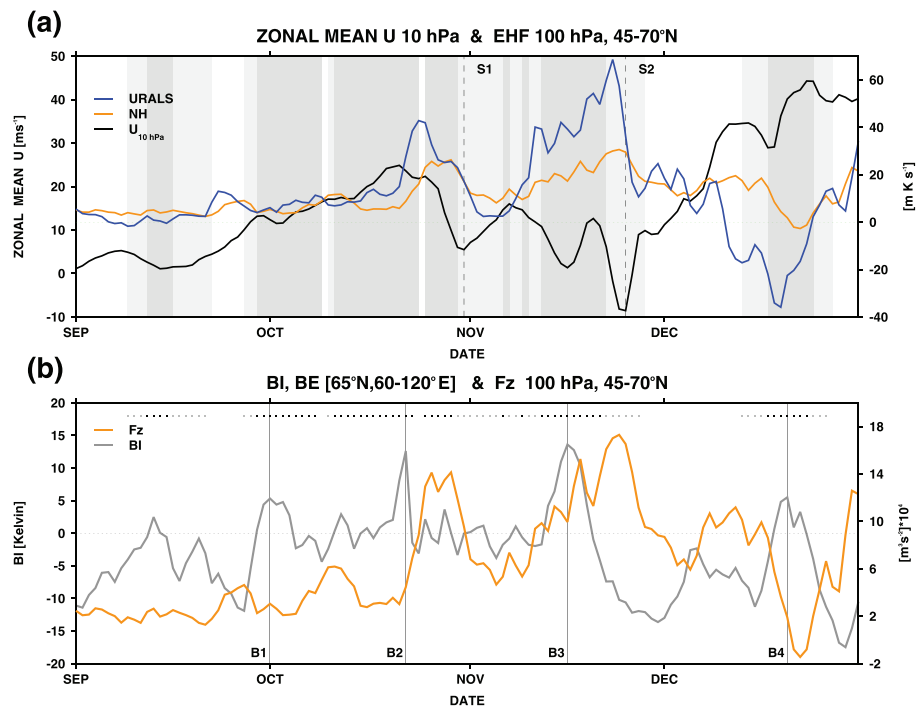


Figure 9. (a) Evolution of daily-mean values of zonal-mean U at 70° N, 10 hPa (black), poleward Eddy Heat Flux (EHF in mKs^{-1}) at 100 hPa averaged within the latitudinal band $45-70^\circ$ N, which is averaged either for the whole Northern Hemisphere (orange) or just the Ural region $40-100^\circ$ E (blue). Vertical dashed lines mark the dates of the major episodes of stratospheric vortex weakening (S1 and S2). (b) Evolution of the Blocking Index (BI in Kelvin, gray curve) averaged over the extended Ural sector (65° N, $60-120^\circ$ E) and the vertical component of the EP flux F_z at 100 hPa, which is averaged within the latitudinal band $45-70^\circ$ N (orange in $m^3s^{-2}10^4$). Light (heavy) gray dots or areas mark dates when Blocking Episodes (BEs) are identified in at least one grid point (in more than 50% of grid-points) within the Ural sector. Vertical lines mark the dates of the four major BEs (B1-B4). The data shown span the period 1 September-31 December 2016.

sea ice loss over the BKS with a lag of about 4 days after the peak of UB intensity. Recently, Chen et al. (2018) investigated the daily evolution of SIC over the BKS for a number of winters (including the winter 2016/2017) and showed that for the winters with more frequent UB, the sea ice loss is greater near the end of the winter due to the cumulative influence of blocking. Thus, the impact of UB on SIC over the BKS was not limited to autumn 2016. Although Chen et al. (2018) established a link between UB and enhancing SIC deficit over the BKS during November 2016 (link C1-B3), they did not provide evidence (their Figure 1b) for the late December 2016 SIC deficit (link B4-C2). In our study, BE was identified to the east of 40° E (Figure 3e), which was not identified by their algorithm. The sea ice loss over the BKS that followed the UB events can be explained by the advection of warm and moist air toward the region; the advection occurs on the western flanks of the blocking ridge (Figures 3a–3d). The developing SIC deficit could be caused not only by sea ice that did not grow or drifted away from the BKS under the strong southwesterly flow but also by the intensification of downward Infrared Radiation (IR; Woods et al., 2013; Woods & Caballero, 2013). Gong and Luo (2017) showed that downward IR increases over the BKS with the establishment of UB due to moisture flux convergence; warm and moist air masses originating from the Atlantic are advected toward the BKS through the Greenland and Norwegian Seas.

5. Troposphere-Stratosphere Coupling

We now investigate the role of the frequent Ural BEs in driving the weakening of the stratospheric polar vortex during autumn 2016 and the possible subsequent surface impact. We explore the evolution of daily-mean values of zonal-mean u and eastward wind tendency due to the divergence of the EP flux ($U_{\text{tend}}DEPF$), both at 10 hPa over the Northern Hemisphere (Figure 8a). The episodes of vortex weakening S1 and S2 developed after phases of vortex deceleration caused by upward flux of wave activity (blue shades). The evolution of the vertical profile of anomalous zonal-mean u at 70° N is shown in Figure 8b. Several negative anomalies

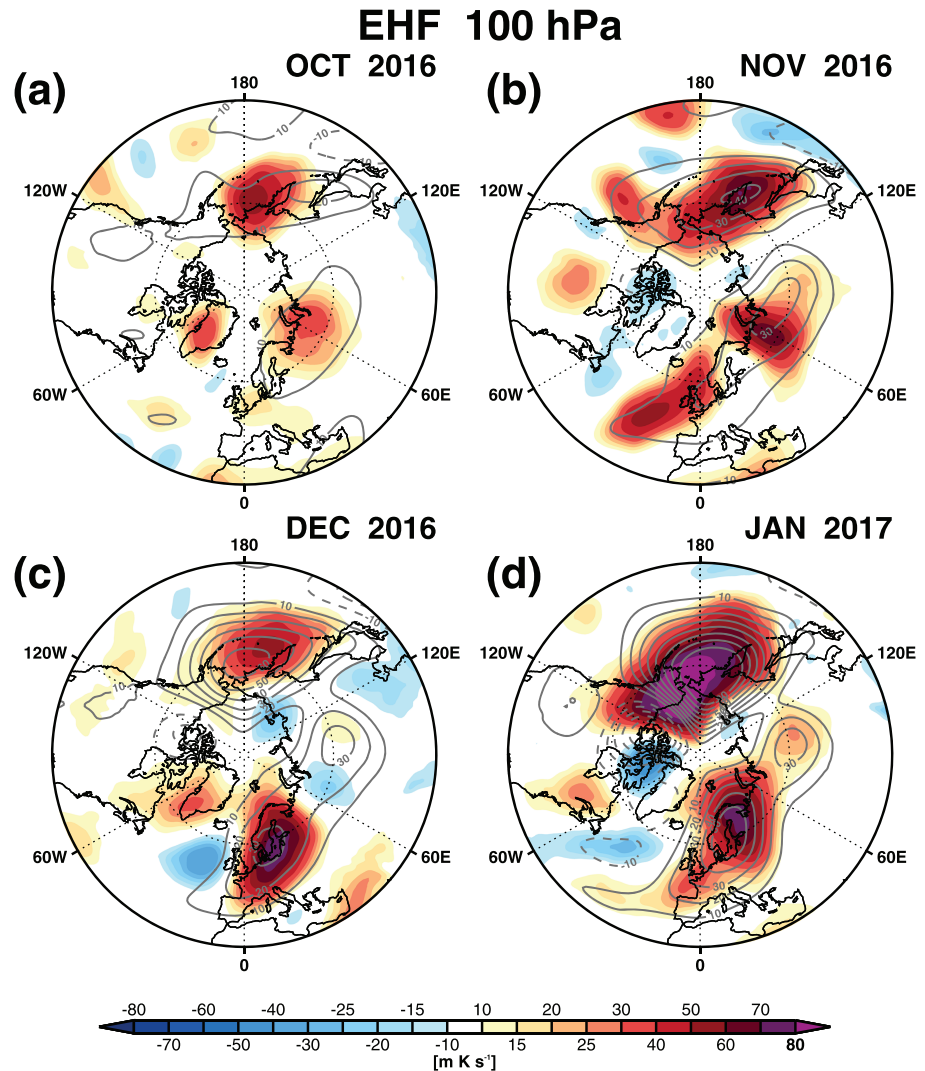


Figure 10. Monthly-mean anomalies of poleward Eddy Heat Flux (EHF, shaded in m K s^{-1}) at 100 hPa for October (a), November (b), and December 2016 (c) and January 2017 (d). The climatology of EHF for the corresponding calendar month is also illustrated (contours). Contour interval is 10 m K s^{-1} with solid (dashed) contours corresponding to positive (negative) values while the zero line is omitted.

(blue shades) are identified throughout the troposphere that are linked to circulation anomalies induced by blocking over Eurasia (B1–B4). Specifically, the episode B2 was followed by negative wind anomalies in the stratosphere that grew with altitude, demonstrating upward propagation of the signal.

Figure 9 sheds additional light on the dynamics of the coupling by illustrating the synchronicity among the episodes of polar vortex weakening and poleward EHF at 100 hPa (a), as well as upward EP flux F_z at 100 hPa and UB activity (b). All fluxes shown are averaged within the latitude band $45\text{--}70^\circ \text{ N}$. UB episodes are associated with an amplified planetary wave pattern that results in enhanced poleward EHF and F_z (orange lines in Figure 9). Each BE was associated with meridional displacements of air masses, with southward intrusions to its east and poleward intrusions to its west (Figures 3a–3d) resulting in maxima of poleward EHF in the vicinity of the blocking. The fluxes averaged specifically over the Ural sector are higher compared with the corresponding zonal-mean fluxes (Figure 9a), which indicates that the UB is an important source of the upward wave activity flux. Further comparison of the monthly-mean anomalies of poleward EHF at 100 hPa to the corresponding monthly climatology (Figure 10) confirms that fluxes over the Urals in October and November are two times greater than average. In December and January, very strong fluxes are found over Europe where blocking occurs and also over the Bering Strait in January 2017.

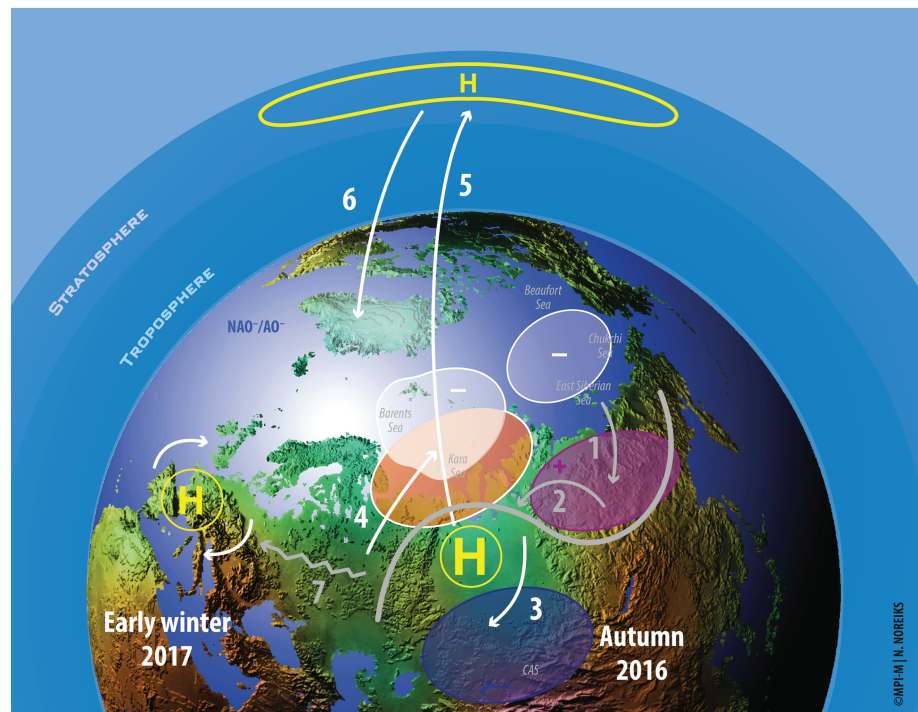


Figure 11. Schematic representation of the dynamics linking the extremes during autumn and early winter 2016–2017. White-shaded areas highlight the negative sea ice anomalies observed over East Siberia Sea (ESS), Chukchi and Beaufort Seas in early autumn, and over Barents-Kara Seas (BKS) in late autumn 2016. Red (blue)-shaded areas highlight the regions of warming (cooling) induced by Ural Blocking. Purple-shaded area delineates the increased snowfall over Siberia, which according to Barnes and Screen (2015) forms due to increased moisture influx following late-summer sea ice loss over the ESS and eventually favors the formation of a wave pattern over Eurasia (gray line). White arrows (3–6) show processes for which we provide evidence in this study and are at play in autumn 2016. Thin gray arrows (1, 2, and 7) show processes that are proposed by other studies (see text). Specifically, arrow 5 highlights the enhanced wave activity injection into the stratosphere that leads to anomalously high geopotential heights over the polar cap (labeled by H) and weakening of the stratospheric vortex. In the troposphere, letter H marks the preferable positions of blocking over the Urals in autumn 2016 and over Europe in early winter 2016–2017.

The peaks of poleward EHF and F_z lagged the ones of Ural BEs by around 10 days (Figure 9b). The slight forward inclination in the temporal evolution of F_z in the upper troposphere and lower stratosphere (Figure S7) is suggestive of the upward propagation of the wave activity flux. Both major episodes of the stratospheric vortex weakening S1 and S2 result from easterly tendency due to divergence of the EP flux at 10 hPa (Figure 8a). Evidently, they were driven by the strong injections of upward wave activity induced by Ural BEs B2 and B3 (Figure 9a). Prior to the major UB episode B3, downward propagation of the easterly anomaly occurred after the severe weakening of the stratospheric vortex S1 (downward arrow in Figure 8b). The anomaly reached the surface within a week, suggesting a downward coupling that might have contributed to the building of the subsequent major episode B3 that in turn amplified the sea ice deficit over the BKS. The above findings are consistent with Takaya and Nakamura (2008) and Peings (2019), who showed that UB activity in November acts to increase the upward flux of planetary waves and thereby weaken the stratospheric vortex in December into January.

6. Summary and Discussion

Autumn and early winter 2016–2017 were characterized by recurring cold surges over Eurasia, exceptionally warm conditions and sea ice loss over the Arctic and an unseasonable weakening of the stratospheric vortex. In this study we present a sequence of dynamical processes that accounts for these extremes (Figure 11). The novelty of our approach is that we highlight the importance of UB in driving all these extremes. We show that in early autumn the sea ice deficit was found over the Beaufort Sea and ESS but by November and December 2016, it had grown to unprecedented levels over the BKS. Successive Ural BEs contributed to the sea ice loss observed in late autumn over the BKS. Each of the BEs induced circulation anomalies that

resulted in cold anomalies to the south and warm anomalies to the north of the blocking ridge (links 3 and 4, Figure 11). Intrusions of warm and moist air resulted in the enhancement of the sea ice loss. Actually, the BKS SIC minimum for 2016 was recorded in mid-November and December, a few days after the two strongest Ural BEs. Additionally, each of the strong Ural BEs drove the intense upward flux of wave activity that resulted in episodes of stratospheric vortex weakening (link 5). Furthermore, at least one case of downward stratosphere-troposphere coupling was identified in mid-November. A downward propagating easterly anomaly was found to reach the surface within 1 week, which could in turn have favored the development of the strongest Ural BE of the season (link 6).

The extreme events observed in autumn 2016 followed a similar course to that described in the conceptual model proposed by Barnes and Screen (2015) and Cohen et al. (2014). This model suggests that Arctic sea ice loss in early autumn, especially over the Chukchi Sea and ESS, may lead to increased moisture inflow and snowfall over Siberia (link 1). The resultant surface cooling can force a stronger trough aloft and a more meandering shape of the polar-front jet over Siberia and thereby possibly favor the building of an upstream ridge over the BKS. Enhanced sea ice deficit and surface heating anomalies migrate from the Chukchi Sea and ESS toward the BKS in November and December. Surface heating over the BKS favors in turn midtropospheric ridging in the BKS and further troughing over East Asia. Thus, increased early autumn snowfall in Siberia and sea ice loss over the BKS in late autumn/early winter can act synergistically to modify the planetary scale configuration over Eurasia (link 2) leading to vertical propagation of Rossby waves and thereby weakening the stratospheric vortex (link 5). However, it should be noted that the effect of snow cover in promoting the occurrence of UB and sudden stratospheric warming is not yet apparent in observations and model simulations (e.g., Henderson et al., 2018).

Accordingly, the enhanced UB activity in October and November 2016 could have resulted from anomalously low SIC in early autumn over the Chukchi Sea and ESS. Evaluation of this hypothesis is the topic of current research. Here, we provide evidence that UB played a key role in amplifying the sea ice loss and warm anomaly over the BKS. Thus, a key result is that the sea ice loss over the BKS in late autumn 2016 was a consequence of the circulation induced by blocking rather than a driver of the blocking activity. This inference is in line with Sorokina et al. (2016) and Peings (2019); the latter study suggested that in November sea ice deficit over the BKS is a response rather than a driver of UB. Such inference may not only hold for this case study as a growing body of recent studies have emphasized the role of UB as an amplifier of Arctic sea ice loss. AA may favor UB occurrence, while the UB-induced warming also enhance the strong background warming over the BKS region (see also Gong & Luo, 2017). It is still an open question, whether the sea ice loss over the BKS exerts any positive feedback forcing that favored the recurrence of the UB events as an upper-level manifestation of the WACS/WACE pattern (Honda et al., 2009; Mori et al., 2014, 2019; Sun et al., 2016). The Polar Amplification MIP (PAMIP; Smith et al., 2019) is expected to bring progress on this question. Multimodel simulations that are forced with various combinations of sea ice representing present-day, preindustrial, and future conditions will be analyzed to investigate whether the sea ice changes over the BKS can influence UB activity and the WACS pattern.

The blocking conditions over Europe and the North Atlantic in late December 2016 and January 2017 can be associated with the negative phase of NAO, which tends to emerge following a weakened stratospheric polar vortex. Following the major blocking episode B3 over the Urals in mid-November, blocking activity spread toward Europe (Figures S2 and S3). Such westward propagation of blocking during winter (link 7, Figure 11) has been documented in previous studies. Chen et al. (2018) described cases of blocking anomalies with sufficient amplitude to propagate westward against the eastward flow (see also Luo et al., 2017; Yao et al., 2017). The weakening of the stratospheric polar vortex in November 2016 might have impacted the midlatitude wave guide on a hemispheric scale by weakening the westerly flow and allowing BE of the Urals to retrogress into Europe in December 2016 and January 2017.

References

- Anagnostopoulou, C., Tolika, K., Lazoglou, G., & Maheras, P. (2017). The exceptionally cold January of 2017 over the Balkan Peninsula: A climatological and synoptic analysis. *Atmosphere*, 8, 252. <https://doi.org/10.3390/atmos8120252>
- Andrews, D. G., Holton, J. R., & Leovy, C. B. (1987). *Middle atmosphere dynamics*. San Diego, California: Academic Press. 489pp.
- Barnes, E. A. (2013). Revisiting the evidence linking Arctic amplification to extreme weather in midlatitudes. *Geophysical Research Letters*, 40, 4734–4739. <https://doi.org/10.1002/grl.50880>

Acknowledgments

The results presented in this study were based on the analysis of ERA-Interim and COBE reanalysis data. Information about how to retrieve the ERA-Interim reanalysis from the European Centre for Medium-Range Weather Forecasts (ECMWF) can be found online (<https://www.ecmwf.int/en/forecasts/datasets/archive-datasets/reanalysis-datasets/era-interim>). Information about how to retrieve the COBE reanalysis data can be found online (http://ds.data.jma.go.jp/tcc/tcc/products/elnino/cobesst_doc.html). The research leading to these results has received funding from the German Federal Ministry of Education and Research (BMBF) through the CLIMPRE InterDec project (FKZ: 01LP1609A; E. T., D. M., J. B., and E. M.), from Japan Science and Technology Agency through the Belmont Forum CRA InterDec (H. N. and J.U.) and from the Japanese Ministry of Education, Culture, Sports, Science and Technology through ArCS Program (H. N. and J.U.). The authors are appreciative of the comments of three anonymous reviewers. Also, they wish to thank Claudia Stephan for providing constructive comments on an earlier version of the manuscript and Norbert Noreiks for preparing the schematic representation in Figure 11.

- Barnes, E. A., Etienne, D. S., Masato, G., & Woollings, T. (2014). Exploring recent trends in Northern Hemisphere blocking. *Geophysical Research Letters*, *41*, 638–644. <https://doi.org/10.1002/2013GL058745>
- Barnes, E. A., & Screen, J. A. (2015). The impact of Arctic warming on the midlatitude jet-stream: Can it? Has it? Will it? *WIREs Climate Change*, *6*, 277–286. <https://doi.org/10.1002/wcc.337>
- Berrisford, P., Hoskins, B. J., & Tyrllis, E. (2007). Blocking and Rossby wave breaking on the dynamical tropopause in the Southern Hemisphere. *Journal of the Atmospheric Sciences*, *64*, 2881–2898.
- Butler, A. H., Seidel, D. J., Hardiman, S. C., Butchart, N., Birner, T., & Match, A. (2015). Defining sudden stratospheric warmings. *Bulletin of the American Meteorological Society*, *96*, 1913–1928. <https://doi.org/10.1175/BAMS-D-00173.1>
- Chen, X., Luo, D., Feldstein, S. B., & Lee, S. (2018). Impact of winter Ural blocking on arctic sea ice: Short-time variability. *Journal of Climate*, *31*, 2267–2282. <https://doi.org/10.1175/JCLI-D-17-0194.1>
- Cohen, J., Screen, J. A., Furtado, J. C., Mathew, B., Whittleston, D., Coumou, D., et al. (2014). Recent Arctic amplification and extreme mid-latitude weather. *Nature Geosciences*, *7*, 627–637. <https://doi.org/10.1038/NNGEO2234>
- Dee, D. P., Uppala, S. M., Simmons, A. J., Berrisford, P., Poli, P., Kobayashi, S., et al. (2011). The ERA-Interim reanalysis: Configuration and performance of the data assimilation system. *Quarterly Journal of the Royal Meteorological Society*, *137*, 553–597. <https://doi.org/10.1002/qj.828>
- Fischer, E. M., & Knutti, R. (2014). Impacts: Heated debate on cold weather. *Nature Climate Change*, *4*, 537–538.
- Francis, J. A., & Vavrus, S. J. (2012). Evidence linking Arctic amplification to extreme weather in mid-latitudes. *Geophysical Research Letters*, *39*, L06801. <https://doi.org/10.1029/2012GL051000>
- Francis, J. A., & Vavrus, S. J. (2015). Evidence for a wavier jet stream in response to rapid Arctic warming. *Environmental Research Letters*, *10*, 014005. <https://doi.org/10.1088/1748-9326/10/1/014005>
- Gerber, E. P., & Manzini, E. (2016). The Dynamics and Variability Model Intercomparison Project (DynVarMIP) for CMIP6: Assessing the stratosphere-troposphere system. *Geoscientific Model Development*, *9*, 3413–3425.
- Gong, T., & Luo, D. (2017). Ural blocking as an amplifier of the Arctic sea ice decline in winter. *Journal of Climate*, *30*, 2239–2254. <https://doi.org/10.1175/JCLI-D-16-0548.1>
- Henderson, G. R., Peings, Y., Furtado, J. C., & Kushner, P. J. (2018). Snow-atmosphere coupling in the Northern Hemisphere. *Nature Climate Change*, *8*, 954–963. <https://doi.org/10.1038/s41558-018-0295-6>
- Hirahara, S., Ishii, M., & Fukuda, Y. (2014). Centennial-scale sea surface temperature analysis and its uncertainty. *Journal of Climate*, *27*, 57–75.
- Honda, M., Inoue, J., & Yamane, S. (2009). Influence of low Arctic sea-ice minima and anomalously cold Eurasian winters. *Geophysical Research Letters*, *36*, L08707. <https://doi.org/10.1029/2008GL037079>
- Horton, D. E., Johnson, N. C., Singh, D., Swain, D. L., Rajaratnam, B., & Diffenbaugh, N. S. (2015). Contribution of changes in atmospheric circulation patterns to extreme temperature trends. *Nature*, *522*, 465–469. <https://doi.org/10.1038/nature14550>
- Hoshi, K., Ukita, J., Honda, M., Iwamoto, K., Nakamura, T., Yamazaki, K., et al. (2017). Poleward eddy heat flux anomalies associated with recent Arctic sea ice loss. *Geophysical Research Letters*, *44*, 446–454. <https://doi.org/10.1002/2016GL071893>
- Inoue, J., Hori, M. E., & Takaya, K. (2012). The Role of Barents Sea ice in the wintertime cyclone track and emergence of a warm-Arctic cold Siberian anomaly. *Journal of Climate*, *25*, 2561–2568. <https://doi.org/10.1175/JCLI-D-11-00449.1>
- Kretschmer, M., Coumou, D., Donges, J. F., & Runge, J. (2016). Sing causal effect networks to analyze different Arctic drivers of mid-latitude winter circulation. *Journal of Climate*, *29*, 4069–4081. <https://doi.org/10.1175/JCLI-D-15-0654.1>
- Kug, J.-S., Jeong, J.-H., Jang, Y.-S., Kim, B.-M., Folland, C. K., Min, S.-K., & Son, S.-W. (2015). Two distinct influences of Arctic warming on cold winters over North America and East Asia. *Nature Geosciences*, *8*, 759–762. <https://doi.org/10.1038/ngeo2517>
- Li, C., Stevens, B., & Marotzke, J. (2015). Eurasian winter cooling in the warming hiatus of 1998–2012. *Geophysical Research Letters*, *42*, 8131–8139. <https://doi.org/10.1002/2015GL065327>
- Luo, B., Luo, D., Wu, L., Zhong, L., & Simmonds, I. (2017). Atmospheric circulation patterns which promote Arctic sea ice decline. *Environmental Research Letters*, *12*, 054017. <https://doi.org/10.1088/1748-9326/aa69d0>
- Luo, D., Xiao, Y., Diao, Y., Dai, A., Franzke, C. L. E., & Simmonds, I. (2016b). Impact of Ural blocking on winter warm Arctic-cold Eurasian anomalies. Part II: The link to the North Atlantic Oscillation. *Journal of Climate*, *29*, 3949–3971. <https://doi.org/10.1175/JCLI-D-15-0612.1>
- Luo, D., Xiao, Y., Yao, Y., Dai, A., Simmonds, I., & Franzke, C. L. E. (2016a). Impact of Ural blocking on winter warm Arctic-cold Eurasian anomalies. Part I: Blocking induced amplification. *Journal of Climate*, *29*, 3925–3947. <https://doi.org/10.1175/JCLI-D-15-0611.1>
- Luo, D., Yao, Y., Dai, A., Simmonds, I., & Zhong, L. (2017). Increased quasi stationarity and persistence of winter Ural blocking and Eurasian extreme cold events in response to arctic warming. Part II: Theoretical explanation. *Journal of Climate*, *30*, 3569–3587. <https://doi.org/10.1175/JCLI-D-16-0262.1>
- McCusker, K. E., Fyfe, J. C., & Sigmond, M. (2016). Twenty-five winters of unexpected Eurasian cooling unlikely due to Arctic sea-ice loss. *Nature Geosciences*, *9*, 838–842. <https://doi.org/10.1038/NNGEO2820>
- Mori, M., Kosaka, Y., Watanabe, M., Nakamura, H., & Kimoto, M. (2019). A reconciled estimate of the influence of Arctic sea-ice loss on recent Eurasian cooling. *Nature Climate Change*, *9*, 123–129. <https://doi.org/10.1038/s41558-018-0379-3>
- Mori, M., Watanabe, M., Shiogama, H., Inoue, J., & Kimoto, M. (2014). Robust arctic sea-ice influence on the frequent Eurasian cold winters in past decades. *Nature Geosciences*, *7*, 869–873. <https://doi.org/10.1038/ngeo2277>
- Nakamura, T., Yamazaki, K., Iwamoto, K., Honda, M., Miyoshi, Y., Ogawa, Y., et al. (2016). The stratospheric pathway for Arctic impacts on midlatitude climate. *Geophysical Research Letters*, *43*, 3494–3501. <https://doi.org/10.1002/2016GL068330>
- Navarro, J. C. A., Ortega, P., Garcia-Serrano, J., Guemas, V., Tourigny, E., Cruz-Garcia, R., et al. (2019). December 2016: Linking the lowest arctic sea-ice extent on record with the lowest European precipitation event on record. *Bulletin of the American Meteorological Society*, *100*(1), S43–S48. <https://doi.org/10.1175/BAMS-D-18-0097.1>
- Newson, R. L. (1973). Response of a general circulation model of the atmosphere to removal of the Arctic ice-cap. *Nature*, *241*, 39–40. <https://doi.org/10.1038/241039b0>
- Nishii, K., Nakamura, H., & Orsolini, Y. J. (2011). Geographical dependence observed in blocking high influence on the stratospheric variability through enhancement and suppression of planetary-wave propagation. *Journal of Climate*, *24*, 6408–6423. <https://doi.org/10.1175/JCLI-D-10-05021.1>
- Ogawa, F., Keenlyside, N., Gao, Y., Koenigk, T., Yang, S., Suo, L., et al. (2018). Evaluating impacts of recent Arctic sea ice loss on the Northern Hemisphere winter climate change. *Geophysical Research Letters*, *45*, 3255–3263. <https://doi.org/10.1002/2017GL076502>
- Orsolini, Y., Senan, R., Benestad, R. E., & Melsom, A. (2012). Autumn atmospheric response to the 2007 low Arctic sea ice extent in coupled ocean-atmosphere hindcasts. *Climate Dynamics*, *38*, 2437–2448. <https://doi.org/10.1007/s00382-011-1169-z>
- Palmer, T. (2014). Record-breaking winters and global climate change. *Science*, *344*, 803–804.

- Parkinson, C. L., & Comiso, J. C. (2013). On the 2012 record low Arctic sea ice cover: Combined impact of preconditioning and an August storm. *Geophysical Research Letters*, *40*, 1356–1361. <https://doi.org/10.1002/grl50349>
- Peings, Y. (2019). Ural blocking as a driver of early-winter stratospheric warmings. *Geophysical Research Letters*, *46*, 5460–5468. <https://doi.org/10.1029/2019GL082097>
- Peings, Y., & Magnusdottir, G. (2014). Forcing of the wintertime atmospheric circulation by the multidecadal fluctuations of the North Atlantic Ocean. *Environmental Research Letters*, *9*, 034018. <https://doi.org/10.1088/1748-9326/9/3/034018>
- Petoukhov, V., & Semenov, V. A. (2010). A link between reduced Barents-Kara sea ice and cold winter extremes over northern continents. *Journal of Geophysical Research*, *115*, D21111. <https://doi.org/10.1029/2009JD013568>
- Screen, J. A., Simmonds, I., Deser, C., & Tomas, R. (2013). The atmospheric response to three decades of observed arctic Sea Ice loss. *Journal of Climate*, *26*, 1230–1248. <https://doi.org/10.1175/JCLI-D-12-00063.1>
- Serreze, M. C., & Francis, J. A. (2006). The Arctic amplification debate. *Climate Change*, *76*, 241–264.
- Smith, D. M., Screen, J. A., Deser, C., Cohen, J., Fyfe, J. C., García-Serrano, J., et al. (2019). The Polar Amplification Model Intercomparison Project (PAMIP) contribution to CMIP6: Investigating the causes and consequences of polar amplification. *Geoscientific Model Development*, *12*, 1139–1164. <https://doi.org/10.5194/gmd-12-1139-2019>
- Sorokina, S. A., Li, C., Wettstein, J. S., & Kvamstø, N. G. (2016). Observed atmospheric coupling between Barents sea ice and the warm-Arctic cold-Siberian anomaly pattern. *Journal of Climate*, *29*, 495–511. <https://doi.org/10.1175/JCLI-D-15-0046.1>
- Sun, L., Perlwitz, J., & Hoerling, M. (2016). What caused the recent “Warm Arctic, Cold Continents” trend pattern in winter temperatures? *Geophysical Research Letters*, *43*, 5345–5352. <https://doi.org/10.1002/2016GL069024>
- Takaya, K., & Nakamura, H. (2008). Precursory changes in planetary wave activity for midwinter surface pressure anomalies over the Arctic. *Journal of the Meteorological Society of Japan. Ser. II*, *86*, 415–427. <https://doi.org/10.2151/jmsj.86.415>
- Tyrlis, E., Tymvios, F. S., Giannakopoulos, C., & Lelieveld, J. (2015). The role of blocking in the summer 2014 collapse of Etesians over the eastern Mediterranean. *Journal of Geophysical Research: Atmospheres*, *120*, 6777–6792. <https://doi.org/10.1002/2015JD023543>
- Tyrrell, N. L., Karpechko, A. Y., Uotila, P., & Vihma, T. (2019). Atmospheric circulation response to anomalous Siberian forcing in October 2016 and its long-range predictability. *Geophysical Research Letters*, *46*, 2800–2810. <https://doi.org/10.1029/2018GL081580>
- Wallace, J. M., Held, I. M., Thompson, D. W., Trenberth, K. E., & Walsh, J. E. (2014). Global warming and winter weather. *Science*, *343*, 729–730. <https://doi.org/10.1126/science.343.6172.729>
- Woods, C., & Caballero, R. (2013). The role of moist intrusions in winter Arctic warming and sea ice decline. *Journal of Climate*, *29*, 4473–4485. <https://doi.org/10.1175/JCLI-D-15-0773.1>
- Woods, C., Caballero, R., & Svensson, G. (2013). Large-scale circulation associated with moisture intrusions into the Arctic during winter. *Geophysical Research Letters*, *40*, 4717–4721. <https://doi.org/10.1002/grl50912>
- Woollings, T. J., Hoskins, B. J., Blackburn, P., & Berrisford, P. (2008). A new Rossby wave-breaking interpretation of the North Atlantic Oscillation. *Journal of the Atmospheric Sciences*, *65*, 609–626. <https://doi.org/10.1175/2007JAS2347.1>
- Yamagami, A., Matsueda, M., & Tanaka, H. L. (2017). Extreme Arctic cyclone in August 2016. *Atmospheric Science Letters*, *18*, 307–314. <https://doi.org/10.1002/asl.757>
- Yao, Y., Luo, D., Dai, A., & Simmonds, I. (2017). Increased quasi stationarity and persistence of winter ural blocking and Eurasian extreme cold events in response to arctic warming. Part I: Insights from observational analyses. *Journal of Climate*, *30*, 3549–3568. <https://doi.org/10.11175/JCLI-D-16-0261.1>
- Zhang, J., Lindsay, R., Schweiger, A., & Steele, M. (2013). The impact of an intense summer cyclone on 2012 Arctic sea ice retreat. *Geophysical Research Letters*, *40*, 720–726. <https://doi.org/10.1002/grl50190>
- Zhang, X., Lu, C., & Guan, Z. (2012). Weakened cyclones, intensified anticyclones and recent cold winter weather events in Eurasia. *Environmental Research Letters*, *7*, 044044. <https://doi.org/10.1088/1748-9326/7/4/044044>